Floating Gate Dosimeter Characterization for Space Applications

De Meyere, William; Shanbhag, Abhimanyu; Menicucci, Alessandra

DOI
10.1109/TNS.2024.3373748

Publication date
2024

Document Version
Final published version

Published in
IEEE Transactions on Nuclear Science

Floating Gate Dosimeter Characterization for Space Applications

William De Meyere, Abhimanyu Shanbhag, and Alessandra Menicucci

***Abstract*— The radiation environment in space can pose a serious risk to both humans and space systems. Widespread and continuous monitoring of this environment is essential to mitigate risks associated with radiation exposure. Miniaturization and use of commercial-off-the-shelf components have enabled significant advances in space technology. These trends can be leveraged to develop innovative radiation sensing and monitoring technologies. However, dosimeters that can effectively measure radiation levels while minimizing their impact on size, power, mass, and cost are required. Floating gate dosimeters (FGDOSs) possess these characteristics, but rigorous testing is needed to ensure their accuracy in spacecraft applications. In this study, we conducted an extensive characterization campaign for an FGDOS chip using a proton beam, increasing the available information on the sensor. The behavior of the dosimeter with respect to resolution, dose rate, beam energy, total ionizing dose (TID), power consumption, annealing, temperature, and single-event effects (SEEs) was experimentally studied. Notably, we observed a previously unseen phenomenon, which we termed "frequency surge" (FS). This phenomenon is likely to have implications for the dosimeter's performance under real spacecraft conditions. Our findings show that the dosimeter is able to combine small power consumption with high dose resolution but also highlight the need for testing against other radiation source types and intensities.**

***Index Terms*— Floating gate dosimeter (FGDOS), radiation monitoring, space environment, total ionizing dose (TID).**

I. Introduction

SPACE radiation has been investigated intensely, but knowledge gaps still exist. Not every region of the space radiation environment has been investigated and radiation models require more data to reduce error margins. Furthermore, continuous monitoring is necessary due to the dynamic behavior of the environment [1].

One of the recent advancements that could facilitate the design of innovative radiation monitoring tools is the floating gate dosimeter (FGDOS). These small, low-cost, yet precise dosimeters could be widely deployed in future space missions. The sensors have possible applications in nuclear and medical research as well. Most of the current research on these dosimeters is being carried out at the European Organization for Nuclear Research (CERN), where the FGDOS is replacing parts of their dosimeter systems [2]. In addition, different versions of the sensor have flown to space, showing promising results [3], [4], [5]. However, in order to confidently use this sensor type in space missions, more clarity is needed concerning its performance. This article aims to contribute to the ongoing development and understanding of the FGDOS. Various characteristics of a commercially available FGDOS chip were experimentally investigated using a proton beam. To advance understanding of the behavior and performance of the FGDOS under conditions that are more representative of spaceflight, unprecedented tests were conducted, which involved irradiation at varying temperatures.

Manuscript received 17 December 2023; revised 26 January 2024 and 28 January 2024; accepted 29 January 2024. Date of publication 6 March 2024; date of current version 16 August 2024. *(Corresponding author: William De Meyere.)*

William De Meyere and Abhimanyu Shanbhag were with the Faculty of Aerospace Engineering, Department Space Engineering, Delft University of Technology, 2629 HS Delft, The Netherlands (e-mail: william.dm@live.be; abhimanyu.shanbhag@gmail.com).

Alessandra Menicucci is with the Faculty of Aerospace Engineering, Department Space Engineering, Delft University of Technology, 2629 HS Delft, The Netherlands (e-mail: a.menicucci@tudelft.nl).

Color versions of one or more figures in this article are available at https://doi.org/10.1109/TNS.2024.3373748.

Digital Object Identifier 10.1109/TNS.2024.3373748

II. Floating Gate Dosimeters

Floating gate transistors have a multilayered gate, with the outer layer closest to the substrate being electrically insulated from the rest of the transistor, thus acting as a potential well. The device can serve as a memory cell but can also be used as a detector for total ionizing dose (TID). Ionizing radiation creates electron–hole pairs in the oxide around the floating gate, and the electrons or the holes, depending on the charge in the gate, migrate toward the gate, effectively discharging it. Another effect of ionizing radiation is the photoemission of charge carriers in the floating gate, i.e., the carriers can get enough energy to cross the insulation boundary when irradiated, also changing the floating gate charge. Since the threshold voltage of these transistors depends on the charge in the floating gate, the amount of radiation dose can be determined by measuring the change in threshold voltage. The monitoring of this shift can be done by measuring the drain current directly or by forcing an equal drain current through both the floating gate transistor and a conventional transistor of equal size, while both are biased with a similar drain–source potential. In the latter case, this results in both transistors having equal gate potential [6], [7], [8].

The FGDOS offers improved sensitivity compared to other typical semiconductor-based dosimeters [2], [9]. Other benefits are their small size, low supply voltage, and the possibility to integrate readout electronics [6], [8]. In addition, the dosimeter can be used in passive mode, meaning that no power supply is needed to detect radiation doses [10]. When power requirements are less stringent, an additional gate bias can be applied to the FGDOS, further improving the sensitivity [11]. Yet, another advantage is their linear response, allowing the sensors to be characterized by just one parameter, the dose sensitivity.

Furthermore, this type of dosimeter can be manufactured in conventional CMOS processes.

A drawback of the sensors is the decrease in sensitivity with increasing TID, similar to MOSFET dosimeters such as the RadFET [12]. The measurement range of these sensors is also limited, and during manufacturing, a tradeoff needs to be made between range and sensitivity. Fortunately, the FGDOS can easily be reset by recharging the floating gate, which effectively extends its total dose range and restores its sensitivity [8]. This means that, by keeping the floating gate charge within limits, the sensor can be operated without leaving its linear range.

The FGDOS investigated in this research is the FGD-03F, a dosimeter chip designed by Sealicon. The chip includes a current-to-frequency converter, resulting in a frequency output corresponding to the amount of charge on the floating gate. Based on the frequency difference before and after irradiation, the amount of dose accumulated in the field oxide can be calculated using the predetermined dose sensitivity of the FGDOS [6], [12], [13]. The FGD-03F chip comes in a QFN32 integrated circuit package containing two dosimeters. Each sensor can be programmed to function with high or low sensitivity, with advertised values of 70 and 10 kHz/Gy(Si), respectively. The exact sensitivities have to be determined via calibration against a known radiation source. Selecting a different sensitivity means that different readout circuitry within the chip is being used. Each sensor is accompanied by a temperature sensor and an additional transistor with a radiation-independent frequency output, used as a reference. This allows for compensation of the temperature-dependent frequency output of the sensor [14].

III. Test Setup

All tests discussed in this article were performed at the Holland Proton Therapy Centre (HPTC), Delft, The Netherlands, from December 2021 to August 2022. The test setup is depicted in Fig. 1. The HPTC cyclotron can provide a proton beam with an energy between 70 and 250 MeV at the device under target (DUT). Both a square and pencil beam shape profile with homogeneity of at least 96% were used. The chosen beam profile followed from the dose rate and beam energy requirements. This did not further affect the tests since the DUT was always completely covered with a homogeneous field. The dose rates ranged from 0.04 to 4.42 Gy/min. All doses mentioned are in silicon. The facility did, however, not provide these directly. Instead, either the particle flux or the dose rate in air was given. To be able to compare the results to other research, these dose rates were then converted to doses in silicon using linear energy transfer (LET). The LET of protons in silicon and air was retrieved from SRIM [15]. The ratio of the LETs is then used to convert the dose rates. Although a more precise conversion using, for example, Monte Carlo simulations could have been performed, the current method was considered to be adequate for this research. An Arduino microcontroller was used to provide power and a clock signal to the sensor chip. Data from the sensors, i.e., frequency output and temperature, were gathered continuously via the same controller with a sample rate of 250 ms. Separate current sensors, type INA219, were used to monitor power consumption of the FGDOS chip. In a later stage, thermoelectric elements and external temperature sensors were added to investigate the temperature-dependent behavior of the sensor. An overview of the test dates and the total TID gathered is depicted in Table I. Four different sensor chips from two different batches, batches A and B, were used during the experiments.

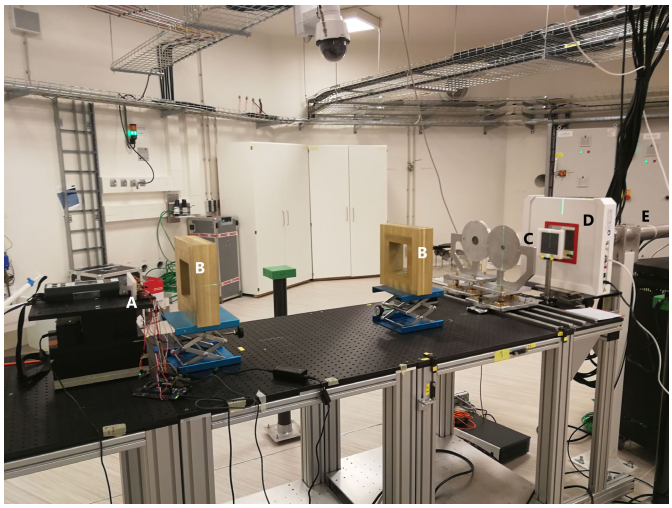

Fig. 1. Test setup. From left to right: DUT (A), collimators (B), scattering ring and sheet (C), beam monitor (D), and proton beam outlet (E).

TABLE I
FGDOS Proton Beam Characterization Summary. Four Chips, Thus Four Sensor Pairs, Were Used: A1, B1, B2, and B3

Sample	Date	Test Purpose	Beam Profile (cm^2)	TID (Gy)
A/1	16/12/2021	Sensitivity determination	4x4 square	>36
A/1	24/02/2022	Beam energy	4x4 square	>32
A/1	08/03/2022	High energy & dose rate	4x4 square	>83
A/1	24/03/2022	Low dose rates	4x4 square	>33
A/1	12/04/2022	Various dose rates Batch A	4x4 square	>32 >216
B/1-2	24/08/2022	Temperature tests	10x10 square	>61
B/3	25/08/2022	Various dose rates Batch B	0.8x0.8 pencil	>140 >201

IV. Sensor Characterization

A. Sensitivity and Linear Range

Although the sensor datasheet mentions a sensitivity of 70 kHz/Gy, previous research demonstrated the actual sensitivity, in high sensitivity mode, to be about 30 kHz/Gy [2], [13], [14]. The sensitivity can be calculated by observing the frequency output of the sensor at two different timestamps. The difference in frequency divided by the amount of TID received between those timestamps then results in a sensor sensitivity in kHz/Gy. In Fig. 2, a typical example of the output of the sensor during a single test run at constant dose rate is shown. The figure shows the frequency decreasing over time, until it crosses a threshold, after the 300-s mark, and the floating gate is recharged, thus increasing the frequency output again. During this test, the sensor was operated outside of the 50–90-kHz linear range mentioned in the datasheet, in order to determine the sensor's behavior over a wider

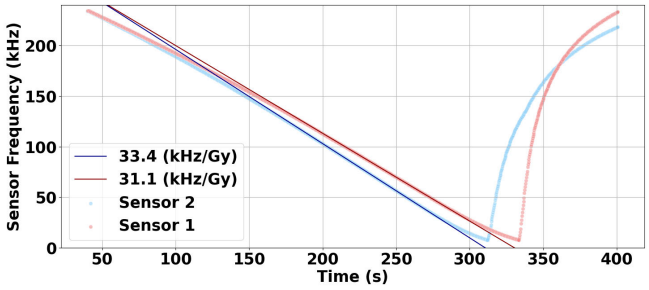

Fig. 2. Output from the FGD-03F from batch A using a beam energy of 70 MeV at DUT and a dose rate of 1.67 Gy/min. The floating gates are recharged after the 300 s mark to reset the frequency output.

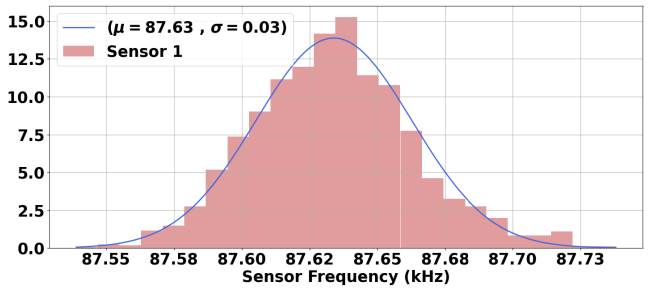

Fig. 3. Histogram of the frequency output of sensor 1 from the chip of batch A for a noise test in high sensitivity mode. A normal distribution is fit on top of the histogram.

TABLE II

SENSITIVITIES FOR BOTH SENSORS IN THE CHIP FROM BATCH A CALCULATED USING LINEAR REGRESSION FOR DIFFERENT PARTS OF THE FREQUENCY RANGE. THE TEST WAS PERFORMED WITH A BEAM ENERGY OF 70 MeV AT DUT AND A DOSE RATE OF 0.78 Gy/min. THE % DIFFERENCE BETWEEN EACH PARTIAL SENSITIVITY AND THE SENSITIVITY CALCULATED OVER THE NOMINAL LINEAR RANGE IS GIVEN AS WELL

Range (kHz)	S1 (kHz/Gy)	Δ (%)	S2 (kHz/Gy)	Δ (%)
50-90	31.3		33.8	
20-40	27.0	-10.90	29.6	-10.41
40-60	30.3	-2.94	33.0	-2.34
60-80	31.2	-0.92	33.8	-1.20
80-100	31.5	-0.12	34.2	0.99
120-100	31.5	0.93	33.9	0.23

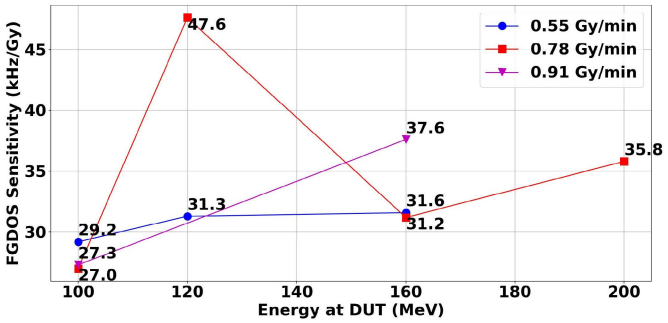

Fig. 4. Sensitivity as a function of energy at different dose rates for a chip from batch B.

range of frequency outputs. The figure also depicts the linear regression lines over the linear range, showing a typical sensitivity over this range of about 32 kHz/Gy. Finally, the figure shows that a wider frequency range can be used when larger deviations from the linear behavior are allowed. In Table II, the sensitivities over the linear range of two sensors are given, as well as the sensitivity per 20 kHz between 20 and 120 kHz.

B. Dose Resolution

Noise tests were performed to determine the resolution, i.e., the smallest detectable dose, of the sensor. The results of such a test are depicted in Fig. 3. In the sensor's datasheet, a noise level of 75 Hz when using a 250-ms measurement window is mentioned [14]. Previous research indicated a minimal detectable frequency of 30 Hz [10]. In [16], it is stated that part of the frequency fluctuations are caused by internal variations in temperature and that the signal can be filtered using a moving average, which resulted in a minimum detectable frequency of 5 Hz. In the current research, however, a noise level of 110 Hz was noted. Applying a moving average to compensate temperature fluctuations, the noise went down to 90 Hz. A noise level of 90 Hz and a sensitivity of 32 kHz/Gy result in a dose resolution of 2.8 mGy. This is better than a typical RadFET sensor, but worse than what is noted in previous studies [12], [17].

A first possible origin of noise is the power supply. The FGDOS is powered through the controller, but the controller itself can be powered through either a conventional charger or via USB. It was noticed that changing the controller's power supply also changes the sensor output frequency by about 0.05%. This indicates the importance of a steady power supply. The controller itself and the included clock signal are possible origins of noise too, as well as the separate current sensors. Noise inherent to the sensor chip may be caused by the analog-to-digital conversion circuitry and readout electronics integrated within the FGDOS chip. The noise caused by the transistor itself has already been investigated in [18].

C. Energy and Dose Rate

In previous research, an increasing trend between beam energy and sensitivity was observed using a prototype of the chip [13]. However, the tests performed in the current research reveal that the relation for the FGD-03F may be weaker than previously reported, as shown in Fig. 4. The cause of the energy dependence is the decrease in LET in silicon of the protons with increasing energy. This has an effect on the charge yield of the incident protons, thus affecting the sensor's sensitivity [19]. The outlier datum point at 47.6 kHz/Gy in the figure is thought to be the result of an anomaly.

In agreement with previous results, it was observed that there is no straightforward dependence of the sensitivity on the dose rate [13], as depicted in Figs. 5 and 6. Although the dose rate affects the sensitivity, an accurate relationship between them cannot be derived from the limited dataset. Tests at lower energies returned similar results. These variations in sensitivity are thought to be a consequence of both annealing and TID effects. Using linear regression on the data depicted in Fig. 7, an indication for the TID-induced degradation can be derived. This results in a degradation rate of about -0.04 (kHz/Gy)/Gy. The total TID accumulated between the

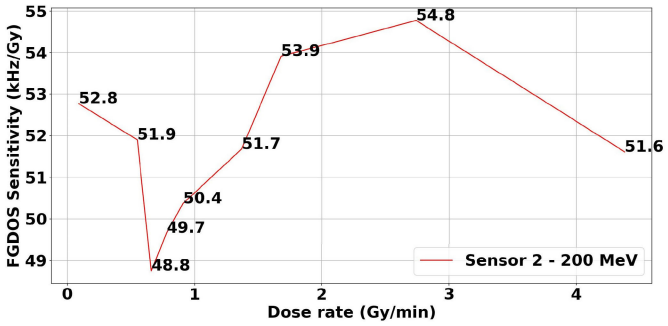

Fig. 5. Sensitivity as a function of dose rate for a sensor from batch A with a beam energy of 200 MeV at DUT.

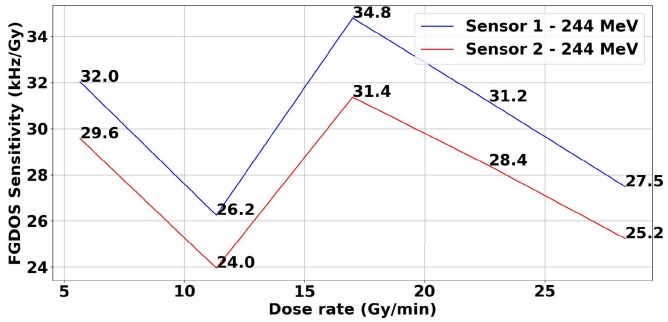

Fig. 6. Sensitivity as a function of dose rate for two sensors from batch B with a beam energy of 244 MeV at DUT.

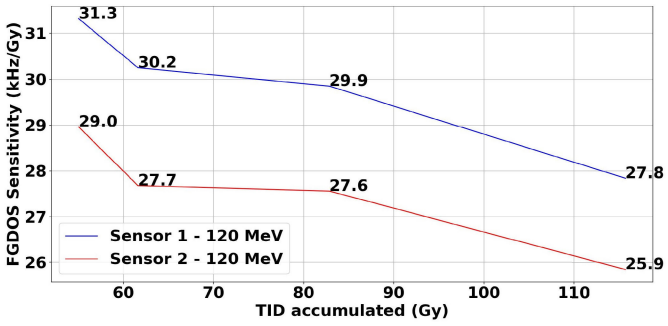

Fig. 7. TID-induced degradation for the B3 sample.

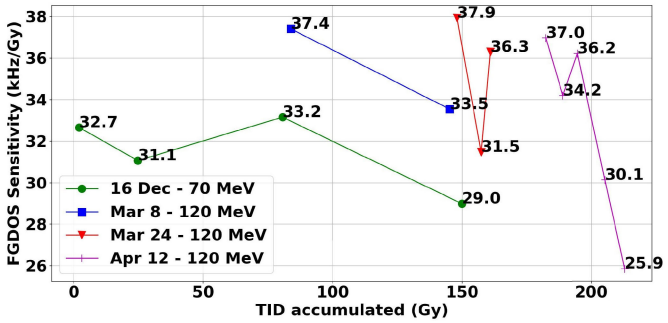

Fig. 8. TID-induced sensitivity degradation in the sensors from sample A1 over multiple test days, at two different beam energy levels. The last three test days all relate to the same sensor.

data points with the lowest and highest dose rate, thus between the outermost data points depicted in Fig. 5, amounts to 47.9 Gy, resulting in a theoretical net sensitivity degradation of 1.9 kHz/Gy. The TID degradation can thus explain the difference between the outermost data points in Fig. 5, but the effect is too small to explain the peaks in sensitivity in the figure. Danzeca et al. [13] also noted that the dose rate dependency changes based on whether the high or low sensitivity mode of the sensor is selected.

D. Sensitivity Degradation

Previous research already indicated that TID causes a degradation of the sensitivity as a result of oxide traps in the field oxide [12], [20]. These traps cause a reduction in the local electric field, thus leading to higher recombination rates and lower sensitivity. In addition, the threshold voltage shift of the readout nMOS transistor, also caused by charge traps, has an influence on the sensitivity. Because of this shift, the floating gate contains less charge after a sensor recharge, resulting in a lower electric field and higher recombination rate. Another effect to take into account is that interface traps in the reading transistor might decrease the channel mobility [12]. A final cause for sensitivity degradation is displacement damage in the field oxide caused by proton collisions [13].

The sensitivity degradation as a function of TID is depicted in Fig. 7. At constant beam energy, the sensitivity changed only slightly until a TID of 85 Gy was reached. Subsequently, it began to decay at an accelerated rate. This is expected to continue until the breakdown point of the digital circuitry of the FGDOS is reached, at around 400 Gy [11], [14].

In Fig. 8, the sensitivity as a function of TID is shown for different energy levels. With a beam energy of 70 MeV, a sensitivity degradation of about 11% can be seen as the TID approaches 150 Gy. With a beam energy of 120 MeV, a degradation of about 31% can be seen as the TID increases from about 85 to 213 Gy. These observations stand in agreement with the findings in [12], where it is noted that the threshold voltage across the MOS readout transistor of the FGDOS begins to fall rapidly after a TID of 200 Gy. The figure also shows that the sensitivity recovers in between test days. An increase in sensitivity was also observed when, on the same test day, there was a delay between consecutive tests. This is further explained in Section IV-E.

The reduction in dose sensitivity was accompanied by a rise in power consumption. It was observed that the power consumption rose linearly from 20 to about 40 mW up to a TID of 165 Gy, but then increased to 80 mW when more than 210 Gy of dose was accumulated. This is depicted in Fig. 9.

E. Short- and Long-Term Annealing

Two mechanisms of annealing are important for the FGDOS. First, a decrease of the frequency was noticed during short breaks in between tests. This is probably caused by the annealing of charge traps in the reading transistor. The traps travel to the substrate, lowering the overall charge stored in the oxide, thus causing a decrease in frequency output. In Table III, an overview of the decrease noticed during such breaks is depicted. For the first tests and at low dose rates, no significant degradation was noticed, which can be expected

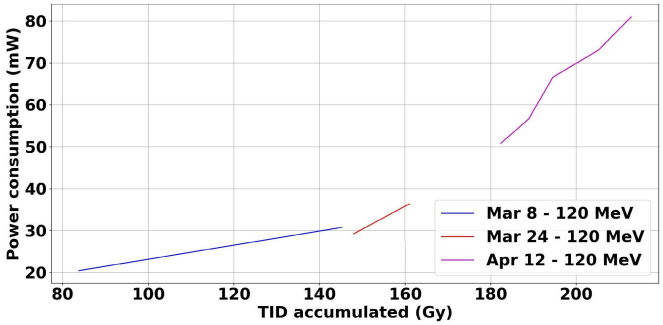

Fig. 9. Power consumption as a function of TID for sensor 2 of batch A.

TABLE III

FREQUENCY DEGRADATION DURING A TEST BREAK. THE DURATION OF EACH BREAK IS NOTED, AS WELL AS THE FREQUENCY CHANGE PER HOUR. SENSITIVITY, ENERGY, AND DOSE RATE ARE THOSE OF THE LAST TEST BEFORE THE BREAK

Energy (MeV)	Sens	Dose rate (Gy/min)	Sensor	Time (min)	dF/dt (kHz/hr)
70	HIGH	0.036	S1	2.0	0
			S2		0
70	LOW	0.778	S1	2.6	2.2
			S2		2.4
70	HIGH	0.149	S1	5.6	2.7
			S2	5.6	2.7

since the low dose rates cause fewer oxide traps. The table shows that higher decreases can be expected right after higher dose rates. In addition, the decrease is lower in low sensitivity mode because the annealing traps have a relatively lower impact on the frequency output. The sensors were also tested again after 29 days. For sensor 1, a decrease from 82.2 to 75.6 kHz was noticed. This agrees with the 4-kHz degradation after five days mentioned in the sensor datasheet [14]. The second effect is the long-term annealing of charge traps in the field oxides, as explained in Section IV-D, resulting in a partial recovery of the sensitivity, as depicted in Fig. 8 [2], [6], [13].

F. Temperature Characteristic

It is known that the behavior of the sensor changes with temperature, due to a temperature-induced shift in the gate-to-source voltage versus drain current characteristic of the readout transistor. A rise in the FGDOS temperature causes the FGDOS frequencies to decrease, while cooling results in a frequency rise. When the FGDOS is subjected to simultaneous irradiation and temperature change, the frequency can either increase, decrease, or remain constant, depending on the relative magnitude of the temperature gradient compared to the dose rate. Two different aspects of coupling between the effects of temperature change and irradiation on sensor frequency values can be observed.

- *Constructive Coupling:* When the temperature of the FGDOS rises, the sensor frequency decreases. Under irradiation, the rising temperature makes for a higher reduction rate of sensor frequency. Hence, based purely on the raw readout from the FGDOS, the combined effect makes it look like the sensor that has an apparent sensitivity higher than the sensitivity at constant temperature. The decrease in sensor frequency becomes nonlinear with respect to time and dose.
- *Destructive Coupling:* When the temperature of the FGDOS decreases, the sensor frequency goes up. This tends to diminish the frequency fall caused by irradiation. Hence, the apparent sensitivity seems to be lower than the sensitivity at constant temperature. Again, the sensor frequency change becomes nonlinear.

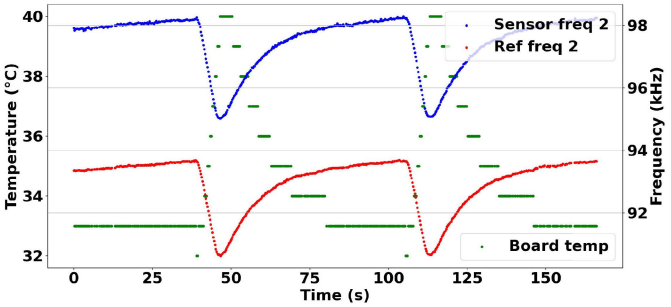

Fig. 10. Frequency output of sensor 2 from a chip of batch B and its reference transistor as a function of time without any radiation present. The temperature of the circuit board on which the sensors were mounted, as measured by the chip's internal temperature sensor, is shown as well. The figure shows a quasi-linear heating temperature profile.

In principle, this coupling should be a linear superposition of the effect of irradiation and the effect of temperature change. The key to decoupling these effects is the reference frequency signal, which is insensitive to radiation but dependent on temperature. The variation with temperature in sensor frequency with respect to the reference frequency is approximately linear, which can be used to compensate the temperature effect on the sensor frequency output [14], [21].

Two FGDOS chips from batch B, mounted on separate circuit boards, were subjected to choreographed temperature profiles in order to observe the effect on the sensor output, both with and without irradiation. A brief description of each temperature profile is provided as follows.

1) *Constant Heating/Cooling Power (Ambient—50 °C):* Constant power was applied to the thermoelectric module on the circuit board for an arbitrary time interval to heat/cool it, irrespective of the starting temperature of the FGDOS chip.
2) *Quasi-Linear (Ambient—40 °C):* Constant heating/cooling power was applied for a short duration such that the resulting rise or fall in temperature was approximately linear, starting from ambient temperature. Fig. 10 shows the effect of a quasi-linear temperature profile, followed by natural convective cooling.
3) *Sawtooth (Ambient—50 °C):* Constant heating/cooling power was applied to change the temperature from ambient to a predefined upper/lower threshold, followed by recovery to ambient temperature by natural convection. This cycle was executed repeatedly for the entire duration of the irradiation run. This profile is depicted in Fig. 11.
4) *Staircase (Ambient—65 °C):* Starting from ambient temperature, the heating/cooling power was modulated to achieve a definite change in the temperature, followed by

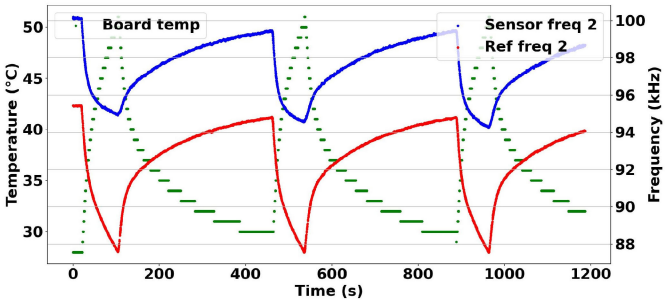

Fig. 11. Frequency output of sensor 2 from a chip of batch B and its reference transistor as a function of time without any radiation present. The temperature of the circuit board on which the sensors were mounted, as measured by the chip's internal temperature sensor, is shown as well. The figure shows a sawtooth heating temperature profile.

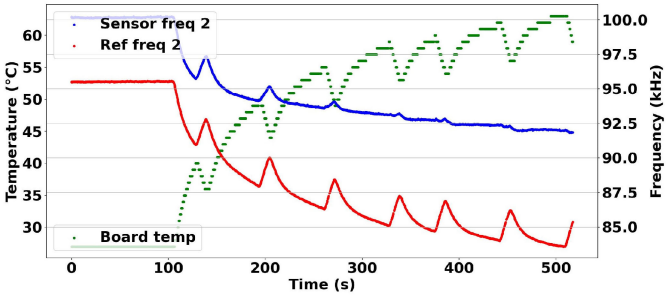

Fig. 12. Frequency output of sensor 2 from a chip of batch B and its reference transistor as a function of time without any radiation present. The temperature of the circuit board on which the sensors were mounted, as measured by the chip's internal temperature sensor, is shown as well. The figure shows a staircase heating temperature profile.

a brief period of natural convective cooling. This cycle was repeated until a predefined maximum/minimum temperature threshold was reached. This profile is depicted in Fig. 12.

5) *Cold Spike (−15 °C—Ambient):* The temperature of the chip was forced to drop abruptly to a subzero minimum by use of a freezer spray, followed by recovery to ambient temperature.
6) *Maximum Heating (Ambient—93 °C):* Maximum power was applied to the thermoelectric module on the circuit board until it reached the peak temperature that could be achieved with the test setup.

For applications in low Earth orbit, a periodic temperature profile can be expected, the characteristics of which depend on the orbit. This profile will include steep temperature gradients when the spacecraft is entering or leaving the sunlit part of its orbit, with relatively stable periods in between. The typical survival temperature range of satellite electronics is −30 °C to 60 °C, but this depends on the mission specifics, such as the location of the sensor and satellite power consumption [22]. Either a staircase profile or consecutive cold spike and maximum heating temperature profiles thus seem to best match typical conditions encountered in low Earth orbit.

For the runs with simultaneous temperature variation and irradiation, the recorded frequencies were compensated using the relationship mentioned previously, and the apparent dose sensitivity was calculated. The apparent sensitivity was

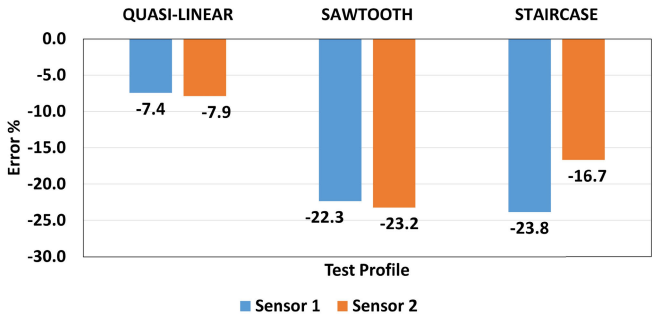

Fig. 13. Effectiveness of temperature compensation for heating in terms of the error in dose sensitivity.

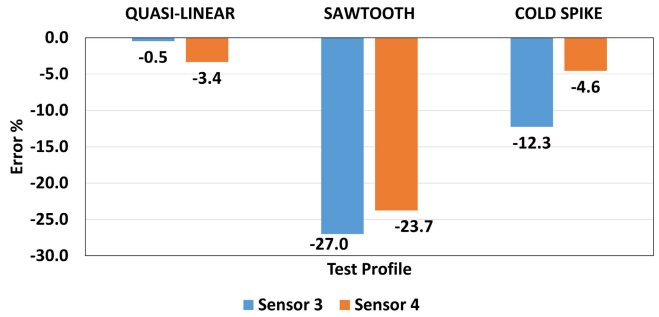

Fig. 14. Effectiveness of temperature compensation for cooling in terms of the error in dose sensitivity.

then compared with a baseline sensitivity, experimentally determined beforehand at constant ambient temperature, to determine the compensation error. Figs. 13 and 14 depict the compensation error with respect to various temperature profiles for the heated and the cooled FGDOS chip, respectively. The compensation effectiveness was observed to be acceptable for the quasi-linear profiles, with computed sensitivity errors within 10%. However, when rapid thermal cycling, steep temperature gradients or gradient reversals are present, the compensation errors climb to higher values, going as high as 25% in some cases. It should be noted that the postprocessing does not account for the change in sensitivity between different runs due to TID or annealing. Another factor, which was not considered, is the change in the frequency versus temperature curve with the working point of the sensor. It was reported by Brucoli et al. [2] that the rate at which the sensor frequency decreases with increasing temperature changes slightly depending on the starting value of the sensor's frequency. Hence, the error values reported in this section should be interpreted as a worst case compensation error.

The compensation error for various thermal profiles reveals that the compensation efficacy suffers when applying steep temperature gradients, gradient reversals, or temperature cycling. Since the temperature variations were induced using conductive heating, this indicates that nonuniform heating/cooling of the FGDOS may result in dissimilar localized heat distributions. As a result, the sensor and reference transistor might be at a different temperature, leading to a degradation in the efficacy of the compensation. This is reinforced by the observation that the sensors encased within the same chip showed slightly different behavior with respect to temperature

variations. Fig. 12 also shows that the frequency from the sensor and reference transistor does not follow the exact same variation, indicating that the local temperature of the sensor and reference transistor may change at different rates when the chip is exposed to sudden external heating or cooling. While this behavior is observed to a small extent for each temperature profile, it was seen to be more pronounced for the staircase profile due to a higher frequency of temperature gradient reversals. Essentially, the difference in thermal response time of various transistors in the chip can lead to a noticeable degradation in the quality of temperature compensation. In addition, Brucoli et al. [2] demonstrated that the temperature characteristic of the reference transistor differs from the characteristic of the sensor transistor. Moreover, the temperature characteristic of the sensor depends on its working point. This means that the compensation can be optimized when using a lookup table where the change in thermal behavior with respect to the working point of the sensor frequency is also accounted for [2], [14]. This approach requires an extensive test campaign to determine the lookup table. Nevertheless, this approach also makes it possible to use a precise temperature sensor instead of a reference transistor to mitigate the temperature dependence of the sensor.

From an operational perspective, the combined effect of temperature variation and irradiation influences the linear range and recharging process of the sensor. Hence, it would be prudent to restrict the range of the sensor such that a sufficient margin is present to account for these effects. It was also observed that the power consumption of the chip does not appear to have an appreciable dependence on the temperature of the chip. This characteristic is favorable for space applications given the adverse thermal conditions and extremes associated with space missions.

The chips were subjected to the most extreme temperature values that could be achieved with the experimental setup. This was done to ascertain the functionality of the FGDOS and to see the effects of extreme variation on sensor frequency compensation. One board was subjected to temperatures ranging from 24 °C to 93 °C, and another board was subjected to temperatures ranging from 24 °C to −15 °C. This part of the test demonstrated that temperature extremes from at least −15 °C to 93 °C could be survived by the FGDOS while providing useful dose measurement data. The chip can thus operate satisfactorily outside its advertised operational temperature range. The absolute maximum allowable temperature range needs to be determined with the help of an experimental setup that can subject the FGDOS to more extreme temperatures than described here.

After the completion of the test runs with irradiation and temperature change, a radiation run was carried out at constant temperature to check whether the repeated thermal stresses resulted in any permanent effects. It was observed that sensor 3 started producing very noisy and irregular sensor frequency values, whereas the reference frequency from sensor 3 remained unaffected. All other sensors being tested did not show any signs of permanent damage caused by either irradiation or temperature change. Due to the limited data, estimations regarding the presence of any definite thermal fatigue or thermally induced residual effects on the FGDOS could not be made.

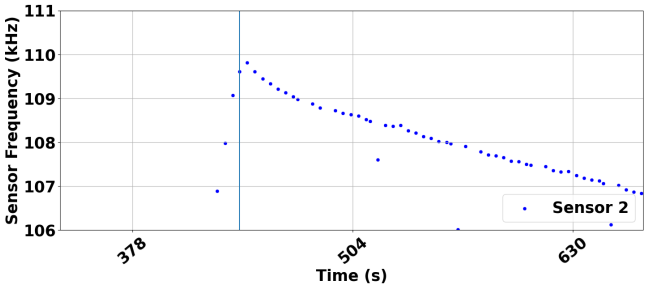

Fig. 15. Sensor frequency as a function of time for a sensor of batch A with the sensor in high sensitivity mode. The vertical line depicts the end of the recharge, after which the sensor frequency still goes up and overshoots its intended endpoint.

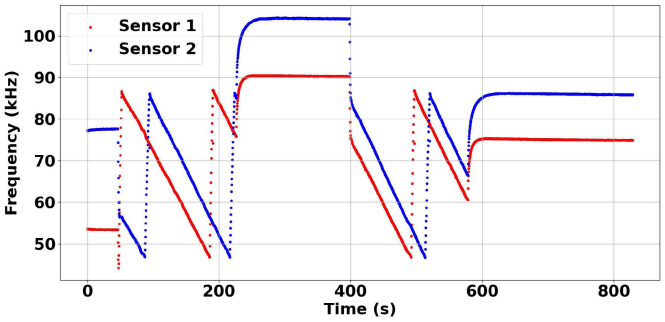

Fig. 16. Sensor frequency as a function of time. The sudden surge, moderation, and drop in frequency can be noticed between 200 and 400 s.

G. Recharge Overshoot

Personal communication with researchers at CERN indicated that the sensor's frequency tends to overshoot right after a recharge. This phenomenon is depicted in Fig. 15. The vertical line in the figure indicates when the recharge process stopped. The sensor frequency still went up after stopping the recharge, after which it dropped and eventually showed linear behavior again. It is assumed that this is caused by an internal capacitive load incorporated in the recharging circuit that has to unload after the end of the recharge process.

H. Frequency Surge

After receiving about 140 Gy of TID, some sensors showed a previously unseen phenomenon, called frequency surge (FS) by the authors. This effect is distributed into three parts: 1) a sudden rise in the sensor frequency post-irradiation; 2) a comparatively gradual moderation of the frequency; and 3) a precipitous drop of the sensor frequency to pre-surge values once irradiation is restarted. All three parts of the FS effect can be seen in Fig. 16.

Owing to the structure and working principle of the FGDOS, the FS can most likely be attributed to its readout circuity. This hypothesis was proposed by CERN researchers as the most probable cause in private communication. For example, the drain current might continue to go up post-irradiation as a result of the release of residual charges. The FS effect has

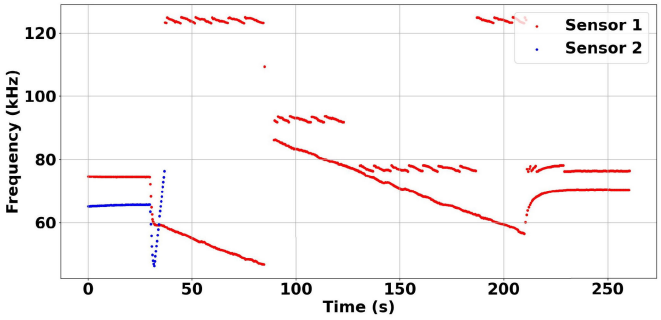

Fig. 17. Effects of an SEE on the observed FGDOS frequency output. An abrupt change on the output can be noticed, beginning at the 40-s mark.

not been noticed before by other researchers. However, it is not an anomaly since further testing conducted on an FGDOS chip from a separate batch produced similar results. Each FGDOS may have a threshold TID, which marks the onset of the FS phenomenon. As long as the TID expected for the operational life or duration of use of an FGDOS is below this threshold, the FS effect may not be a relevant concern. The need for a viable explanation as to the onset of the FS effect at high TID levels calls for further investigation into this phenomenon.

I. Single-Event Effects and Other Anomalies

The FGDOS is known to occasionally exhibit large variations in temperature and frequency output data, which has been attributed to single-event effects (SEEs) in the memory registers [13]. These SEEs can be filtered out and their effect is automatically resolved due to the registers being refreshed on each read cycle. However, it was noticed that due to SEEs, the frequency output of a sensor could also give abnormal spikes or just stop completely. These effects are depicted in Fig. 17. The anomaly was not resolved until the sensor was reset via power cycling. It was also noticed that these erroneous frequency outputs could trigger a recharge in the chip, resulting in the sensors being recharged to frequencies far outside the linear range. Because the issue is resolved after a power cycle, it is assumed that these unexpected values are all due to radiation effects in the registers. Another anomalous behavior shown by the FGDOS was the breakdown of a sensor during large swings in temperature, as well as an inversion of the temperature-dependent characteristic of the sensor frequency. The direct cause for this anomaly could not be identified.

The aforementioned anomalies do not provide a possible explanation of the FS phenomenon. First, memory register errors are resolved after a read cycle, while the surge persists after a read cycle. Furthermore, the FS effect could also not be mitigated by power cycling the chip.

J. Discrimination and Mitigation of Various Effects

The aforementioned effects of temperature, beam energy, TID, and annealing on sensor sensitivity can all occur simultaneously. It is thus difficult to discriminate between these effects and their relative influence on the sensitivity. Although it is not always possible to completely separate their effects, several steps were taken during the characterization campaign to minimize or completely eliminate them whenever possible. First, except for the specific temperature characterization runs, the temperature during the tests remained relatively constant. This is, however, based on the output of the chip's temperature sensor, which has a limited precision of 1 °C. Second, the degradation effect caused by TID was only compared between test runs with equal dose rates and beam energy levels. The decrease in sensitivity between different test days is influenced by long-term annealing effects, but this influence was not quantified.

For practical applications of the FGDOS, the aforementioned effects might need to be compensated, in order to acquire more accurate and reliable dosimetry measurements. The TID-induced degradation in sensitivity can be compensated using a calibration curve or a lookup table acquired during pre-flight characterization [10]. As described in Section IV-F, the effect of temperature variation on sensor frequency can be compensated using the corresponding reference frequency with a lookup table-based approach. Short-term annealing and long-term annealing can be differentiated on the basis of the time scale at which the sensor frequency is observed to vary. Given the lack of understanding surrounding the actual cause of the FS effect, it can be challenging to compensate for it. As such, it would be prudent to operate the FGDOS only until the aforementioned threshold TID is reached. As mentioned in Section IV-I, most SEEs are automatically resolved once the registers are refreshed at the next read cycle. However, other SEEs may require a reset of the FGDOS. As such, monitoring of the sensor output and the implementation of some elementary housekeeping functionalities is required to power cycle the FGDOS in case anomalous data are observed.

K. Sensor Variability

For sensors embedded in the same FGDOS chip, it was observed that the trends in sensitivity as a function of TID, dose rate, beam energy, and temperature were largely the same over the entire test campaign. It should be noted that the sensors exhibit slightly different sensitivities as well as reference frequencies, most probably a result of variations in the manufacturing process. Sensor output could, however, differ significantly when one of the sensors suffers from an SEE in its circuitry. As noted previously by Brucoli et al. [2], a small variation in the properties of the sensors from different batches, in addition to intra-batch variations, is to be expected. In the scope of the current study, FGDOS chips from two different batches were used and no significant differences were noted besides their sensitivity.

V. Conclusion

First, it was found that the measured dose sensitivity of the chip agreed well with the sensitivity noted in previous research. In addition, the sensitivity outside of the linear range was determined to differ only slightly from the sensitivity within the range. Second, the dose resolution of the sensor chip was verified through noise measurements. Although the

current setup had a worse dose resolution compared to previous research, it still outperformed typical RadFETs. Third, an increase in sensitivity with increasing particle energy has been noted, but there was no conclusive effect of dose rate on sensitivity. Subsequently, the TID-induced degradation of the sensitivity was tested for, as well as two annealing phenomena. It was demonstrated that the sensitivity gradually decreases with increasing TID, although part of the lost sensitivity is recovered via the long-term annealing process. In addition, the effect of temperature variation on the sensor's output and the effectiveness of temperature compensation were experimentally studied. The experiments show that dose measurements can be made under adverse thermal conditions. However, the compensation deteriorates under high-temperature gradients. Next, the FS phenomenon was described, but the underlying cause of the surge remains unknown. Finally, the occurrence of SEEs and other anomalies was discussed, followed by remarks on how the effects of various anomalies and known variations such as TID degradation can be identified and accounted for when postprocessing measurement data.

A. Future Research

In the future, a precise comparison between the response of the FGDOS to different types of radiation should be performed [13]. Moreover, the response of the sensor to very low dose rates, on the order of several μGy/hr, delivered overextended time intervals has not been tested. Since one of the advantages of the sensor is its high dose resolution, the origin of the relatively high noise levels encountered in this research could be further investigated. Another phenomenon, which has not been investigated, yet is the dependence of short- and long-term annealing on the temperature of the FGDOS. Further investigation of the sensor's behavior under different types of radiation might lead to the discovery of new sensor characteristics. For instance, it has been demonstrated that the sensor can also be used as a heavy ion charge yield measurement device [23].

Based on an overview of the testing and characterization efforts that have been invested in the development of the FGDOS, various design and operation-related improvements can be envisioned. First, the dose sensitivity of the floating gate could be increased since this directly impacts the resolution and precision of dosimetric measurements. However, this could imply an undesired increased dependence of sensitivity on TID. Rizzo et al. [11] demonstrated sensitivity enhancement by applying an electric field over the floating gate and field oxide. To compensate the effect of temperature, it is apparent that the addition of a more precise temperature sensor in the FGDOS chip would allow for more precise temperature compensation using a lookup table. Another design improvement lies in the thermal design such that heat is distributed more evenly across the volume of the chip, thereby reducing the compensation inaccuracies that were described in Section IV-F. The results obtained from the temperature profiles that were used in this study can serve as input for improving the thermal design of FGDOS chips as well as payloads utilizing the FGDOS. Operational improvements primarily stem from the application for which the chip is to be used. For instance, Zimmaro et al. [24] have suggested ways to curb power consumption using standby and passive mode configurations, in context of long-term radiation monitoring. For space applications, operational improvements should mainly revolve around reducing noise for accurate measurements in very low dose rate environments as well as reducing the effect of temperature variations. To increase capabilities of the FGDOS beyond basic time-resolved dosimetry, detailed Monte Carlo radiation transport studies could be conducted to understand the response of the sensor to various radiation types, energies, fluxes, and dose rates.

B. Future Applications

The FGDOS can be used as a miniaturized radiation monitor on-board spacecrafts, as proven by the 4M Lunar Flyby Mission [3]. A recently developed version of the Space RadMon device, a satellite payload developed by CERN, will also incorporate an FGDOS [4]. Another example is the SATDOS-1 payload hosted by the Austrian CubeSat PRETTY [5], which launched October 2023 and will conduct measurements of TID in low Earth orbit using an FGDOS. Considering the challenging size, mass, power, and cost constraints that are associated with miniaturized spacecraft platforms, the FGDOS characteristics make it a promising technology for missions involving Earth orbit constellations as well as deep space spacecraft. On the surface of the Moon, the capabilities of the FGDOS will be demonstrated by the first mission of the hexapod nano-rover called Lunar Zebro [25]. The scientific goal of Lunar Zebro's first mission is to measure radiation in the lunar environment. As its primary science payload, the Lunar Zebro rover will carry on-board two FGDOS units to investigate the ionizing radiation environment through time-resolved dosimetry measurements at multiple locations on the lunar surface. The payload will feature a distributed sensing architecture, whereby the first FGDOS unit will be housed within the chassis of the rover, whereas the second unit will be mounted on the exterior. This will result in minimal shielding of primary ionizing radiation for the second FGDOS.

ACKNOWLEDGMENT

The authors would like to thank the Holland Proton Therapy Centre, Delft, The Netherlands, for providing test facilities, and Dr. Salvatore Danzeca, Dr. Matteo Brucoli, and Alessandro Zimmaro from the European Organization for Nuclear Research (CERN) for providing feedback on experimental results and utilization of the floating gate dosimeter (FGDOS).

REFERENCES

[1] O. P. Verkhoglyadova et al., "Addressing gaps in space weather operations and understanding with small satellites," *Space Weather*, vol. 19, no. 3, Mar. 2021, Art. no. e2020SW002566.

[2] M. Brucoli et al., "Floating gate dosimeter suitability for accelerator-like environments," *IEEE Trans. Nucl. Sci.*, vol. 64, no. 8, pp. 2054–2060, Aug. 2017.

[3] J. Cesari, A. Barbancho, A. Pineda, G. Ruy, and H. Moser, "Floating gate dosimeter measurements at 4M lunar flyby mission," in *Proc. IEEE Radiat. Effects Data Workshop (REDW)*, Jul. 2015, pp. 93–96.

[4] CERN. *Space RadMon*. Accessed: Apr. 15, 2023. [Online]. Available: https://kt.cern/aerospace/spaceradmon

[5] C. Tscherne et al., "Development of a miniaturized reference dosimeter payload for SmallSat applications," in *Proc. 21st Eur. Conf. Radiat. Effects Compon. Syst. (RADECS)*, Sep. 2021, pp. 1–6.

[6] M. Alvarez, C. Hernando, J. Cesari, A. Pineda, and E. Garcia-Moreno, "Total ionizing dose characterization of a prototype floating gate MOSFET dosimeter for space applications," *IEEE Trans. Nucl. Sci.*, vol. 60, no. 6, pp. 4281–4288, Dec. 2013.

[7] E. Garcia-Moreno et al., "Floating gate CMOS dosimeter with frequency output," *IEEE Trans. Nucl. Sci.*, vol. 59, no. 2, pp. 373–378, Apr. 2012.

[8] M. Garcia-Inza, S. Carbonetto, and A. Faigon, "MOS devices and integrated circuits for ionizing radiation dosimetry: A review," in *Proc. Argentine Conf. Electron. (CAE)*, Feb. 2020, pp. 31–40.

[9] A. Karmakar, J. Wang, J. Prinzie, V. De Smedt, and P. Leroux, "A review of semiconductor based ionising radiation sensors used in harsh radiation environments and their applications," *Radiation*, vol. 1, no. 3, pp. 194–217, Aug. 2021.

[10] M. Brucoli et al., "Investigation on passive and autonomous mode operation of floating gate dosimeters," *IEEE Trans. Nucl. Sci.*, vol. 66, no. 7, pp. 1620–1627, Jul. 2019.

[11] M. Rizzo, M. Brucoli, S. Danzeca, A. Masi, À. Pineda, and B. Servera Mas, "An enhanced sensitivity operation mode for floating gate dosimeters," *IEEE Trans. Nucl. Sci.*, vol. 69, no. 8, pp. 1876–1883, Aug. 2022.

[12] M. Brucoli et al., "Investigation on the sensitivity degradation of dosimeters based on floating gate structure," in *Proc. 17th Eur. Conf. Radiat. Effects Compon. Syst. (RADECS)*, 2017, pp. 287–290.

[13] S. Danzeca et al., "Characterization and modeling of a floating gate dosimeter with gamma and protons at various energies," *IEEE Trans. Nucl. Sci.*, vol. 61, no. 6, pp. 3451–3457, Dec. 2014.

[14] Sealicon. (Jun. 2021). *FGD-03F*. [Online]. Available: https://www.sealiconmicro.com/sealicon-products-documentation-3

[15] J. F. Ziegler. *SRIM—The Stopping and Range of Ions in Matter*. Accessed: Jan. 8, 2022. [Online]. Available: http://www.srim.org/

[16] M. Brucoli, "Total ionizing dose monitoring for mixed field environments," Ph.D. dissertation, Institut d'Electronique et des Systèmes (IES), Univ. Montpellier, Montpellier, France, 2018.

[17] R. Ferraro, S. Danzeca, M. Brucoli, A. Masi, M. Brugger, and L. Dilillo, "Design of a radiation tolerant system for total ionizing dose monitoring using floating gate and RadFET dosimeters," *J. Instrum.*, vol. 12, no. 4, Apr. 2017, Art. no. C04007.

[18] J. Cesari et al., "Study of floating gate MOS structures to improve the noise and sensitivity as radiation dosimeter," in *Proc. 17th Eur. Conf. Radiat. Its Effects Compon. Syst. (RADECS)*, 2017, pp. 291–294.

[19] M. Wind, P. Beck, and A. Jaksic, "Investigation of the energy response of RADFET for high energy photons, electrons, protons, and neutrons," *IEEE Trans. Nucl. Sci.*, vol. 56, no. 6, pp. 3387–3392, Dec. 2009.

[20] T. R. Oldham and F. B. McLean, "Total ionizing dose effect in MOS oxides and devices," *IEEE Trans. Nucl. Sci.*, vol. 50, no. 3, pp. 483–499, Jun. 2003.

[21] M. Brucoli et al., "A complete qualification of floating gate dosimeter for CERN applications," in *Proc. 16th Eur. Conf. Radiat. Effects Compon. Syst. (RADECS)*, 2016, pp. 306–309.

[22] V. L. Pisacane, "Spacecraft thermal control," in *Fundamentals of Space Systems*. Oxford, U.K.: Oxford Univ. Press, 2005, pp. 423–464.

[23] M. Brucoli et al., "Heavy-ion charge yield measurement by floating gate dosimeters," in *Proc. 21st Eur. Conf. Radiat. Effects Compon. Syst. (RADECS)*, Sep. 2021, pp. 168–171.

[24] A. Zimmaro et al., "Testing and validation methodology for a radiation monitoring system for electronics in particle accelerators," *IEEE Trans. Nucl. Sci.*, vol. 69, no. 7, pp. 1642–1650, Jul. 2022.

[25] J. M. Tejeda, P. Fajardo, M. K. Verma, and C. Verhoeven, "The complete set of thermo-mechanical-radiation methods, simulations and results for a swarm of nanorovers deployed on the Moon's surface (Lunar Zebro mission)," *Adv. Astronaut. Sci. Technol.*, vol. 5, no. 4, pp. 317–334, May 2022.